Proceedings of the Combustion Institute, Volume 29, 2002/pp. 2001–2008

LARGE-EDDY SIMULATION OF PREMIXED TURBULENT COMBUSTION USING A LEVEL-SET APPROACH

H. PITSCH AND L. DUCHAMP DE LAGENESTE
Center for Turbulence Research
Stanford University
Stanford, CA 94305-3030, USA

In the present study, we have formulated the G equation concept for large-eddy simulation (LES) of premixed turbulent combustion. The developed model for the subgrid burning velocity is shown to correctly reflect Damköhler's limits for large- and small-scale turbulence. From the discussion of the regime diagram for turbulent premixed combustion, it is shown that given a particular configuration of flow parameters, changes in the LES filter width result in changes along constant Karlovitz number lines. The Karlovitz number is chosen as the horizontal axis to construct a new regime diagram for LES of premixed turbulent combustion, where changes in the filter width are represented by vertical lines. In addition, some new regimes appear in the new diagram, which are related to the numerical treatment. An important conclusion is that changes in the filter width cannot result in changes of the combustion regime among the corrugated flamelets, thin reaction zones, and broken reaction zones regimes. This is a consistency requirement for the model, since the choice of the filter width cannot change the fundamental combustion mode. With decreasing filter width, changes from corrugated to wrinkled flamelets, or in general to a laminar regime, are possible. In applying the model in a numerical simulation of a turbulent Bunsen burner experiment, it is shown that the results predict the mean flame front location, and thereby the turbulent burning velocity, and the influence of the heat release on the flow field in good agreement with experimental data.

Introduction

Large-eddy simulation (LES) of premixed turbulent combustion is now considered to be a promising field. It has the potential to improve predictions of reacting flows over classical Reynolds-averaged Navier-Stokes (RANS) approaches, which lack precision, especially in complex geometry or, for instance, for swirling flows with recirculation.

Since the reaction zone thickness of premixed flames in typical engineering devices is thin, with a characteristic length scale much smaller than a typical LES filter width, chemical reactions occur only on the subgrid scales. Hence, these must be modeled entirely. Different methods have been proposed to model premixed combustion in LES.

One approach is to artificially thicken the flame by increasing the diffusivity [1–3]. The flame can then be resolved on the LES grid and a subgrid chemical closure is not necessary. To correct the effect on the flame propagation speed, the chemical source term must be modified by the use of so-called efficiency functions obtained from direct numerical simulations (DNS) [4]. This method has already been applied with some success. However, the main drawback of this method is that it can change the principle underlying physical process from a transport-controlled to a chemistry-controlled combustion mode.

The basic idea in flamelet models is that of a thin flame sheet. This assumption leads to two important consequences. First, if the flame, or at least the reaction zone, is thinner than the small turbulent scales, the structure of the flame or the reaction zone remains laminar. Second, within the thin flame, the gradients are very high, and hence, the chemical reactions are balanced by diffusive transport. As an implication of the latter, in a turbulent flow, these terms cannot be modeled independently. In the flamelet model, the flame is replaced by an interface moving with a laminar burning velocity s_L, which can be expressed in terms of the molecular diffusivity D and the characteristic chemical time scale t_c as $s_L \sim (D/t_c)^{1/2}$, thereby capturing the balance of molecular transport and the chemistry.

In a turbulent flow, the local mass burning rate can then be modeled if the laminar burning velocity and the local flame surface area per unit volume are known. Hawkes and Cant [5], for instance, have proposed a flamelet model for LES based on a reaction progress variable. In this model, a transport equation for the subgrid flame surface density is solved. Since this formulation relies on the laminar burning velocity, the model can only be applied in the corrugated flamelet regime.

A different formulation of flamelet models is the level-set method, where the instantaneous flame

front is treated as an interface, represented by an isosurface of a scalar field G, defined by $G = G_0$. This isosurface is convected by the velocity field **u,** while it propagates normal to itself with the laminar burning velocity. An equation describing the evolution of this scalar field, the so-called G equation, has been proposed by Williams [6]. For turbulent flows, this equation is only valid if the flame thickness, comprising the inert preheat zone and the thin reaction zone, is small compared to the small turbulent scales. This is commonly called the corrugated flamelets regime. For this regime, a closure for the transport equations of the Reynolds-averaged G and its variance has been provided by Peters [7].

If the flame thickness is larger than the small turbulent scales, but the reaction zone remains thinner, the reaction zone structure still remains laminar, and only the transport in the preheat zone is changed by the turbulence. This has been called the thin reaction zones regime [8].

Different formulations of flamelet models for LES based on the G equation have been proposed, for the corrugated flamelets regime, for instance, by Chakravarthy and Menon [9] and for the thin reaction zones regime by Kim and Menon [10].

Peters [8] has provided a transport equation for G, valid in both the corrugated flamelets and the thin reaction zones regime as

$$\rho \frac{\partial G}{\partial t} + \rho \mathbf{u} \cdot \nabla G = \rho s_L |\nabla G| - \rho D \kappa |\nabla G| \quad (1)$$

where t is the time, ρ is the density, **u** is the velocity vector in the unburned mixture, and κ is the curvature of an isosurface of G. In this equation, the first term on the right-hand side is the propagation term involving the laminar burning velocity, which is dominant in the corrugated flamelets regime, and the second term is the curvature term, most important in the thin reaction zones regime. Since the laminar burning velocity is defined only at the flame surface, equation 1 is only valid at G_0, and the G field outside of this surface must be defined differently. Note that since equation 1 has no diffusion term, the solution at G_0 does not depend on the definition of the remaining field.

A Reynolds-averaged form of equation 1 has been derived by Peters [8]. Also an analytic model for the turbulent burning velocity, which appears as an unclosed term in the mean G equation, is provided from a transport equation for the flame surface area ratio.

In the following, using arguments similar to those of Peters [8], a model for LES of premixed combustion based on the G equation and valid for both the corrugated flamelets and the thin reaction zones regime will be presented. The model will be validated using data from a turbulent Bunsen burner experiment by Chen et al. [11]. Numerical results from the LES are compared with measured velocity and temperature data for the cold and the reactive flow.

Regime Diagram in Large-Eddy Simulation

Regime diagrams for premixed turbulent combustion in terms of velocity and length scale ratios have been proposed by Borghi [12] and other authors. A recent version by Peters [8] introduces the thin reaction zones regime, limited by the criterion $Ka_\delta = 1$, where Ka_δ is Karlovitz number based on the reaction zone thickness. This considerably extends the flamelet regime beyond the Klimov-Williams criterion, for which flamelets exist only if the turbulent Karlovitz number Ka is smaller than unity.

In addition to the Karlovitz number, which is the ratio of the time scales of the laminar flame and the Kolmogorov eddies, the turbulent Reynolds number, Re, and the turbulent Damköhler number, Da, appear in the discussion of premixed turbulent combustion and should therefore be introduced here. For LES, these numbers can be defined with the characteristic subgrid velocity fluctuation v'_Δ and the LES filter width Δ as

$$Re_\Delta = \frac{v'_\Delta \Delta}{s_L l_F}, \; Da_\Delta = \frac{s_L \Delta}{v'_\Delta l_F}, \; Ka = \frac{l_F^2}{\eta^2} \quad (2)$$

where l_F is the laminar flame thickness and η is the Kolmogorov length scale. It is important to note that, while changes of the filter width result in changes in the Reynolds and the Damköhler number, the Karlovitz number is independent of the filter width. Changes in the filter width therefore proceed at constant Karlovitz number.

The regime diagram by Peters [8] is given as v'/s_L as a function of l/l_F, where v' is the turbulent velocity fluctuation at the integral length scale l. In LES, the integral length scale must be replaced by a characteristic subgrid length scale, which can be given by the filter width. It follows that the location in the regime diagram depends on the LES filter size. The objective here is to discuss the influence of the filter size on the location in the regime diagram and to develop a new regime diagram for LES, which allows to clearly distinguish between changes of the turbulence/chemistry interaction and the numerical treatment in an LES.

The transfer rate of turbulent kinetic energy ε is inertial range invariant. Hence, the scaling for ε in terms of a velocity and a length scale can be employed at any length scale within the inertial subrange. The appropriate relation is given here at the integral length scale and at the filter scale

$$\varepsilon = \frac{v'^3}{l} = \frac{v'^3_\Delta}{\Delta} = \frac{(s_L l_F)^3}{\eta^4} \quad (3)$$

The third relation in equation 3 is the scaling at the

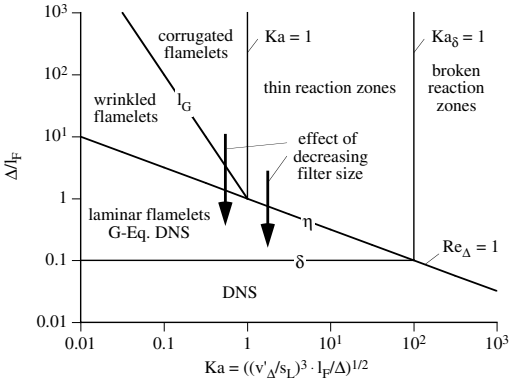

FIG. 1. Regime diagram for LES of turbulent premixed combustion.

Kolmogorov scale $\varepsilon = \nu^3/\eta^4$, where the kinematic viscosity ν with the assumption of constant Schmidt number has been replaced by $\nu = D = s_L l_F$. Combining equation 3 and the Karlovitz number in equation 2 leads to

$$Ka^2 = \frac{l_F}{s_L^3}\,\varepsilon = \left(\frac{v'_\Delta}{s_L}\right)^3 \frac{l_F}{\Delta} \tag{4}$$

Equation 4 has two important implications. The first relation in equation 4 shows that the Karlovitz number only depends on the laminar flame scales and the turbulent kinetic energy transfer rate ε and is hence independent of the filter width. Because of this, the second part of equation 4 provides a relation for v'_Δ/s_L as a function of the filter width. Since the Karlovitz number is not affected by the filter width, it demonstrates how variations in the filter width influence the subgrid velocity fluctuation. Equation 4 can be inserted into equation 2 to obtain for the Reynolds number and the Damköhler number

$$Re_\Delta = Ka^{2/3}\left(\frac{\Delta}{l_F}\right)^{4/3} = Ka^{-2}\left(\frac{v'_\Delta}{s_L}\right)^4 \text{ and}$$

$$Da_\Delta = Ka^{-2/3}\left(\frac{\Delta}{l_F}\right)^{2/3} = Ka^{-2}\left(\frac{v'_\Delta}{s_L}\right)^2 \tag{5}$$

Since the only quantity independent of the filter width is the Karlovitz number, it seems convenient to use the Karlovitz number instead of the length scale ratio to construct a regime diagram for LES. As a second axis either the velocity ratio v'_Δ/s_L or the length scale ratio Δ/l_F can be chosen. Here we will use Δ/l_F, since this clearly reveals the influence of the filter width.

The new regime diagram can be constructed from the relations given in equation 5 and is shown in Fig. 1. It includes the same physical information as Peters' diagram [8], but in addition it reveals some new regimes, which are related to the numerical treatment. This diagram also has the advantage that the consequences of changing the filter width become evident. This is indicated in Fig. 1, showing, for instance, that a change in the filter width cannot change the combustion regime across the Klimov-Williams criterion ($Ka = 1$) or the Peters criterion ($Ka_\delta = 1$). Therefore, in the new regime diagram, changes in the horizontal direction correspond to changes in the turbulence/chemistry interaction at constant filter width, while changes in the vertical direction correspond to changes in the filter width at constant physical parameters.

Starting from the corrugated flamelets regime, a smaller filter width can decrease the subgrid fluctuations such that $v'_\Delta < s_L$ when the filter width becomes smaller than the Gibson scale l_G, thereby changing the modeled part of the combustion process to the wrinkled flamelet regime. The corrugation of flamelets would then occur at the resolved scales and would not appear in the subgrid modeling. Although the subgrid part of the flame in this regime has a completely laminar structure, the flow field still reveals subgrid turbulence. If from here, or from the thin reaction zones regime, the filter width is decreased even further, also the subgrid part of the flow field becomes laminar when $\Delta < \eta$. In this so-called laminar flamelets regime, the turbulence is resolved by the simulation, but the reaction zone thickness is still smaller than the filter width. However, if the G equation according to equation 1 would be used in a simulation, all relevant length scales would be resolved in this regime. This regime can therefore also be referred to as the G equation DNS regime. If in this regime or starting from the broken reaction zones regime the filter width is further decreased to a value smaller than the reaction zone thickness δ, then also the length scale of the reaction zone is resolved and the simulation constitutes a DNS, also if a temperature or progress variable equation rather than the G equation is solved.

Governing Equations

We consider the low Mach number approximation of the Navier-Stokes equations. To achieve a proper description of the flow field, the filtered equations for mass and momentum conservation must be solved. The filtered density appearing in these equations has to be provided by the combustion model.

Filtered G Equation

Following a procedure similar to that of Peters [13], an equation for the filtered G equation valid in both the corrugated flamelets and the thin reaction zones regime can be derived as

$$\bar\rho\,\frac{\partial \tilde G}{\partial t} + \bar\rho\tilde{\mathbf{u}}\cdot\nabla\tilde G = \bar\rho s_T|\nabla\tilde G| - \bar\rho D_t\tilde\kappa|\nabla\tilde G| \tag{6}$$

Here, the bar denotes a spatial filtering and the tilde

a spatial Favre filtering. The double prime appearing below stands for the Favre fluctuations. This equation is only valid at the flame surface, outside of which $\tilde{G}$ must be defined differently. Here, for convenience, the flame is assumed to be at $G_0 = 0$ and the remaining part of the $\tilde{G}$ field will be determined to be a signed distance function, negative in the unburned and positive in the burned gases.

The turbulent burning velocity s_T appearing in equation 6 has been introduced as

$$(\bar{\rho} s_T)\ |\nabla \tilde{G}| = (\rho s_L)\bar{\sigma} \tag{7}$$

where $\bar{\sigma}$ is the flame surface area ratio, which is yet unknown and must be modeled. Modeling of the conditional velocity appearing in equation 6 is described in Ref. [13].

Turbulent Burning Velocity

Similarly to Peters [14], an equation for the subgrid variance of G corresponding to equation 6 can be derived as

$$\bar{\rho}\frac{\partial \widetilde{G''^2}}{\partial t} + \bar{\rho}\tilde{\mathbf{u}} \cdot \nabla \widetilde{G''^2} + \nabla \cdot (\bar{\rho}\mathbf{u}''\widetilde{G''^2}) = 2\bar{\rho}D_t\,(\nabla \tilde{G})^2 - \bar{\rho}\tilde{\omega} - \bar{\rho}\tilde{\chi} \tag{8}$$

Since equation 6 is only defined to be valid for $\tilde{G} = G_0$ and the variance can only be defined with the mean, also equation 8 can only be used at $\tilde{G} = G_0$. The fluctuation G'' represents the departure of the instantaneous flame front from the mean flame front location. In equation 8, the turbulent production term has been modeled using a gradient transport assumption, where D_t is the turbulent diffusivity. The last two terms denote the kinematic restoration and the scalar dissipation, respectively. Both result in the attenuation of the variance of G and act on the small scales. Therefore, the scaling for these terms developed by Peters [8] in a Reynolds-averaged context can also be used here. In particular, it has been shown that the kinematic restoration should be proportional to the mean propagation and independent of the small scales [7], and the scalar dissipation must involve a molecular diffusivity [8]. This leads to

$$\tilde{\omega} = c_2\,(s_L\bar{\sigma})^2\,\frac{C_v\Delta}{v''_\Delta} \text{ and } \tilde{\xi} = c_3 D\bar{\sigma}^2 \tag{9}$$

Here, c_2 and c_3 are proportionality factors. The subgrid time scale has been determined from the subgrid velocity fluctuation and the sub-grid length scale $C_v\Delta$, where C_v is the Smagorinsky coefficient determined by a dynamic model as described in Moin et al. [15]. Assuming that in the scalar variance equation the production term balances the attenuation terms leads with equations 9 and 7 to an analytic expression for the turbulent burning velocity

$$\frac{s_T - s_L}{s_L} = b_3\sqrt{\frac{D_t/D}{1 + \dfrac{b_3^2}{b_1^2 Sc_t}\dfrac{C_v\Delta}{l_F}\dfrac{s_L}{v_\Delta}}} = \frac{v'\Delta}{s_L}\,b_3\sqrt{\frac{Da_\Delta/Sc_\Delta}{1 + \dfrac{b_3^2}{b_1^2 Sc_\Delta}\,Da_\Delta}} \tag{10}$$

The laminar burning velocity has been added to achieve the correct limit for laminar flows. The constants c_2 and c_3 have been determined such that the expression for the turbulent burning velocity for $C_v\Delta/l_F \gg v'_\Delta/s_L$ or $Da_\Delta \gg 1$ results in Damköhler's large-scale limit

$$\frac{s_T - s_L}{s_L} = b_1\frac{v'_\Delta}{s_L} \tag{11}$$

and for $C_v\Delta/l_F \ll v'_\Delta/s_L$ or $Da_\Delta \ll 1$ in Damköhler's small-scale limit [16]

$$\frac{s_T - s_L}{s_L} = b_3\sqrt{\frac{D_t}{D}} \tag{12}$$

The resulting expressions are $c_2 = 2/(Sc_\Delta b_1^2)$ and $c_3 = 2/b_3^2$, where the constants b_1 and b_3 have been taken from Peters [14] to be $b_1 = 2.0$ and $b_3 = 1.0$. The subgrid diffusivity, the subgrid Schmidt number Sc_Δ, and the subgrid velocity fluctuation can all be determined by dynamic models. Here, following the suggestion of Pitsch and Steiner [17], a constant Schmidt number of $Sc_\Delta = 0.5$ is assumed. The subgrid diffusivity is determined from $D_t = C_v\Delta v'_\Delta/Sc_\Delta$.

Since the subgrid burning velocity is a function of the filter size, it is interesting to discuss the respective dependency. Inserting equation 4 into equation 11 shows that $(s_T - s_L)/s_L \sim (\Delta/l_F)^{1/3}$, implying that in the large-scale limit a doubling in the filter size only leads to an about 25% increase in the burning velocity. For the small-scale limit, equations 5 and 12 lead to $(s_T - s_L)/s_L \sim (\Delta/l_F)^{2/3}$, which would result in an approximately 50% change, if the filter size was doubled.

As shown in the discussion above, the subgrid burning velocity essentially includes two parts, the kinematic restoration, important in the corrugated flamelets regime, and the dissipation, important in the thin reaction zones regime. As equation 10 shows, the transition depends on the Damköhler number and thereby on the filter width. This seems to be in contrast with the earlier finding that the combustion regime is independent of the filter width. In the corrugated flamelet regime, the turbulent length scale is much larger than the flame thickness, and hence, the dissipation, representing curvature effects, is present, but cannot be important. However, the curvature becomes important,

when the turbulent length scale becomes of the order of the flame thickness. In the corrugated flamelet regime, decreasing the filter size reduces the largest scales which must be modeled. When the filter width is reduced such that it becomes comparable to the flame thickness, the effects of curvature become important for the subgrid burning velocity. However, it is easy to see from equation 5 that the Damköhler number cannot become smaller than unity in the corrugated or the wrinkled flamelet regime. Thereby, even if curvature effects become increasingly important, s_T still remains dominated by the kinematic restoration.

Evaluation of the Filtered Density

To solve the momentum equations, the filtered density must be computed from the combustion model. Peters [14] has suggested an algorithm in the Reynolds-averaged context for adiabatic simulations. The algorithm used in this study is similar, but extended to account for possible heat losses to the burner, which have been found to be important in the experiment considered for the present simulations. The present formulation also accounts for the mixing of the postflame region with the coflowing air.

If the flame thickness is small compared to the filter width, the temperature can be assumed to be discontinuous at the flame, changing from the constant unburned to the adiabatic flame temperature. This assumption can then also be made for the density.

To account for heat losses, an equation for the filtered enthalpy $\tilde{h}$ is solved. The enthalpy is defined to include the heat of formation and is hence a conserved quantity, except for heat losses at walls and radiative heat losses, the latter of which have been neglected here. To account for inert mixing with the coflowing air, also an equation for a filtered mixture fraction $\tilde{Z}$ is solved. The mixture fraction is defined to be zero in the coflowing air and unity in the premixed jet. Both of these equations have no chemical source terms and, hence, do not require any chemistry closure model.

The density is assumed to be a function of the mixture fraction, the enthalpy, and G only. The instantaneous density can then be determined as

$$\rho(Z,\, h_1,\, G) = \begin{cases} \rho_u(Z) & \text{if } G < 0 \\ \rho_b(Z,\, h_1) & \text{otherwise} \end{cases} \qquad (13)$$

where in the unburned gases, the density is determined by inert mixing given by $\rho_u(Z) = [Z/\rho_1 + 1 - Z/\rho_2]^{-1}$, and ρ_2 and ρ_1 are the densities in at $Z = 0$ and $Z = 1$, respectively. In the burned gases, the density is given by the solution of a steady-state flamelet library, describing the mixing of hot stoichiometric gases with cold coflowing air. For the simulation of steady-state flamelets, the enthalpy varies linearly with the mixture fraction. For the test case considered below, heat losses occur only in the pilot flame, where $Z = 1$. Therefore, only h_1 appears as a parameter in the flamelet equations, and the density can be described as $\rho = \rho_b(Z, h_1)$.

The evaluation of the filtered density then follows the presumed pdf approach as described in Peters [14].

Numerical Simulation

Experimental Setup

As a test problem for the model presented in the previous section, the so-called flame F_3, experimentally investigated by Chen et al. [11], has been chosen. The experimental setup consists of a stoichiometric premixed methane/air flame stabilized by a large pilot flame. Both incoming streams, the main jet and the pilot, have the same composition and are surrounded by a coflowing air stream. The nozzle diameter D of the main stream is 12 mm. The pilot stream issues through a perforated plate (1175 holes of 1 mm in diameter) around the central nozzle with an outer diameter of 5.67 D. The main stream is turbulent with a jet Reynolds number based on the inner nozzle diameter and a bulk velocity of $U_0 =$ 30 m/s of $Re = 23{,}486$. Based on the estimated characteristic length and time scale given in Chen et al. [11], the velocity and length scale ratios can be determined to be $u'/S_L = 11.9$ and $l/l_F = 13.7$. This leads to a Karlovitz number of $Ka = 11.1$, indicating that flame F_3 is located well within the thin reaction zones regime, but still far from the broken reaction zones regime.

Large-Eddy Simulation

The computer code used in this study has been developed at the Center for Turbulence Research by Pierce and Moin [18,19]. The filtered low Mach number approximation of the Navier-Stokes equations is solved in cylindrical coordinates on a structured staggered mesh. The numerical method is a conservative, second-order finite-volume scheme. Second-order semi-implicit time advancement is used, which alleviates the CFL restriction in regions where the grid is refined. Details of the numerical method can be found in Pierce [19] and Akselvoll and Moin [20]. The flamelet library has been computed using the GRI-MECH 2.11 chemical reaction mechanism [21].

To ensure sufficient regularity of the $\tilde{G}$ field away from the $\tilde{G}^0$ surface, $\tilde{G}$ is defined in the whole domain as a distance function. The constraint $|\nabla\tilde{G}| = 1$ needs to be enforced at each time step by a so-called reinitialization procedure. The numerical procedure used here has first been described in Sussman et al.

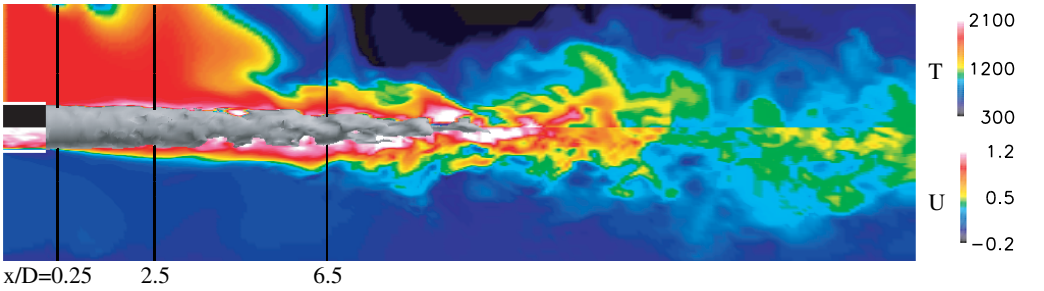

FIG. 2. Instantaneous flame position (gray surface), temperature distribution (top part), and axial velocity distribution (bottom part)

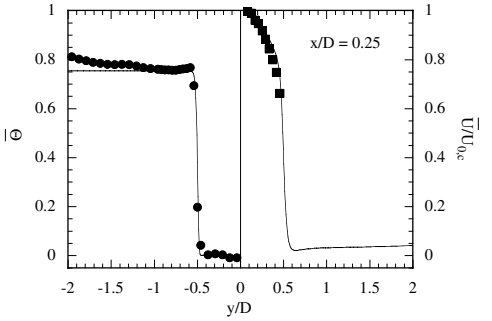

FIG. 3. Time-averaged temperature and axial velocity at $x/D = 0.25$. Lines, simulation; symbols, experimental data.

[21] and was later extended by Russo and Smereka [22].

Grid and Boundary Conditions

The computational domain extends to 20 D downstream of the nozzle and 4 D in the radial direction. The LES grid is 296 × 64 × 64, corresponding to approximately 1.2 million cells. At the inflow boundary, instantaneous velocities extracted from a separate LES of a fully developed pipe flow are prescribed. Convective conditions [19] are prescribed at the outflow boundary, while traction-free conditions [23] are imposed on the lateral boundaries to allow entrainment of fluid into the domain. The enthalpy in the inflow streams has been prescribed to match the experimental temperature at the first experimental station, which is very close to the nozzle at $x/D = 0.25$.

Results and Discussion

An example of the instantaneous flame surface is shown in Fig. 2. The acceleration of the burned gases behind the flame front caused by the heat release is illustrated by the instantaneous field of the axial velocity given in the bottom part of the figure. The top part of Fig. 2 shows the corresponding temperature field. The highest temperatures can be observed in the region behind the instantaneous flame front.

Due to the consumption of the unburned mixture, the mean flame front position is converging toward the centerline at farther downstream positions. The computed, time-averaged axial position, where the fuel is completely consumed, is at approximately $x/D = 9.0$, which is in good agreement with the experimental value of $x/D = 8.5$ given in Chen et al. [11]. This result shows that the model for the subgrid turbulent burning velocity s_T leads to a reasonable prediction of the averaged flame location.

Quantitative results are compared to experimental data in Figs. 3–6. To judge the performance of the combustion model and also to discuss the effect of heat release, results from a cold flow simulation will be discussed first. Figures 4 and 5 show radial profiles of the time averaged axial velocity at $x/D = 2.5$ and 6.5. The turbulent kinetic energy at these positions is shown in Fig. 6. The agreement for all data is very good, providing confidence in the ability of LES to describe this flow correctly and particularly in the proper treatment of the inflow conditions provided from the experiments.

The mean radial profiles of temperature and axial velocity very close to the nozzle at $x/D = 0.25$ are compared to experimental data in Fig. 3. The agreement is quite good and is shown here only to demonstrate that the inflow conditions have been chosen appropriately. In the adiabatic case the maximum non-dimensional temperature, defined as $\tilde{\Theta} = (\tilde{T} - T_1)/(T_b - T_1)$, where T_b is the adiabatic flame temperature, should be $\Theta = 1.0$. However, because of the strong heat losses to the pilot nozzle, the maximum temperature in the pilot flame is only $\Theta \approx 0.8$.

The mean radial profiles of temperature and axial velocity for the reactive case are also shown in Figs. 4 and 5. Significant differences can be observed in the velocity predictions compared to the cold flow case, for which the mean axial velocity at the centerline decreases much faster than for the reactive

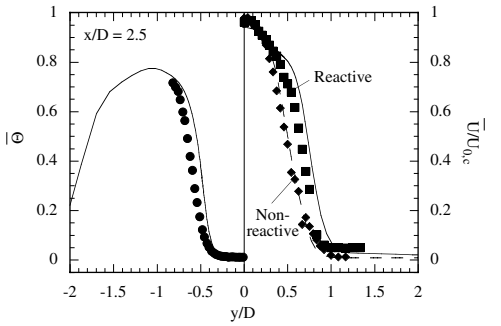

FIG. 4. Time-averaged temperature and axial velocity at $x/D = 2.5$. Lines, simulation; symbols, experimental data.

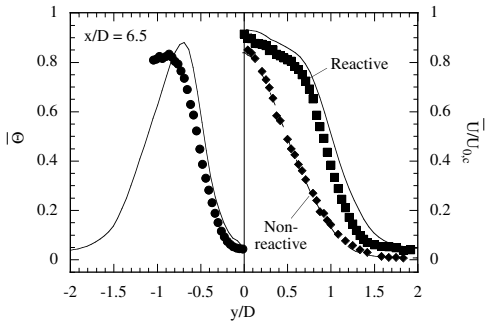

FIG. 5. Time-averaged temperature and axial velocity at $x/D = 6.5$. Lines, simulation; symbols, experimental data.

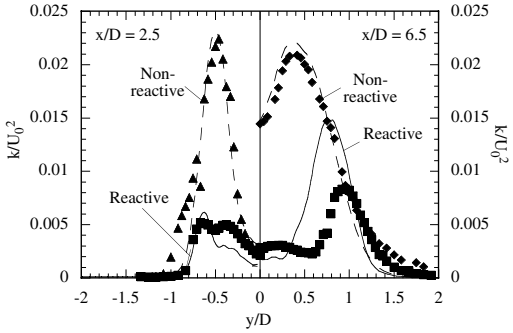

FIG. 6. Turbulent kinetic energy at $x/D = 2.5$ and 6.5. Lines, simulation; symbols, experimental data.

case. This also reveals much broader radial profiles compared to the cold flow case. The main reason for this is the acceleration induced by the heat release. This effect is captured by the simulation in good agreement with the experimental data.

The temperature profiles generally overestimate the experimental data slightly, but the agreement is still reasonable. The strong cooling influence of the broad pilot flame can be observed at $x/D = 2.5$. At $x/D = 6.5$, the cold coflowing air stream also becomes important.

Figure 6 shows the radial profiles of the turbulent kinetic energy k for the cold and the reactive simulation. As for the mean velocity, the evolution of k at the centerline is found to be very different in both cases. For the cold flow case, the turbulent kinetic energy is increasing in the downstream direction and reaches a maximum at $x/D = 8.5$, which is not shown here, whereas k stays approximately constant for the reactive case. This result confirms that combustion strongly influences transport of turbulence toward the centerline by preventing radial transport of the turbulent kinetic energy produced in the shear layers. Although some discrepancies remain, this important result, also observed in the experiments [11], is well reproduced by the simulation. In the reactive case, the turbulent kinetic energy profiles reveals two maxima, one on the burned side and one on the unburnt side of the mean flame position. The radial location of both peaks is well predicted. However, the maximum values are generally overpredicted.

Conclusions

In conclusion, the G equation model has been shown to be well suited for applications in LES. The model for the subgrid burning velocity presented here correctly represents Damköhler's large-scale and small-scale turbulence limits. The influence of the LES filter width on the model predictions has been discussed in terms of the regime diagram for turbulent premixed combustion. It has been shown that the Karlovitz number is independent of the LES filter width. The implication is, for instance, that changes of the filter width cannot change the combustion regime, but can account for the correct transition of the subgrid burning velocity to the laminar burning velocity when the filter width becomes smaller than the Kolmogorov length. Although the choice of the filter width can potentially change the subgrid burning velocity from the Reynolds-averaged turbulent to the laminar burning velocity, the dependence has been shown to be weak. This is a benefit for LES, since then the exact choice of the filter width becomes less important.

In the application of the model to a turbulent Bunsen burner experiment, reasonable agreement with the experimental data indicates that the turbulent burning velocity and the influence of the heat release on the flow field are correctly represented by the model.

Acknowledgments

The authors gratefully acknowledge funding by Snecma Moteurs and by the US Department of Energy within the ASCI program. We also thank C. D. Pierce for supplying the LES solver and N. Peters for comments and discussion.

REFERENCES

1. Poinsot, T., Veynante, D., and Candel, S., *J. Fluid Mech.* 228:561–606 (1991).
2. Colin, F., Veynante, D., and Poinsot, T., *Phys. Fluids* 12(7):1843–1863 (2000).
3. Nottin, C., Knikker, R., Boger, M., and Veynante, D., *Proc. Combust. Inst.* 28:67–73 (2000).
4. Angelberger, C., Veynante, D., and Egolfopoulos, F., *Flow Turbulence Combust.* 65:205–222 (2000).
5. Hawkes, E. R., and Cant, R. S., *Proc. Combust. Inst.* 28:51–58 (2000).
6. Williams, F. A., "Turbulent Combustion," in *The Mathematics of Combustion* (J. D. Buckmaster, ed.), Society for Industrial and Applied Mathematics, 1985, pp. 197–318.
7. Peters, N., *J. Fluid Mech.* 242:611–629 (1992).
8. Peters, N., *J. Fluid Mech.* 384:107–132 (1999).
9. Chakravarthy, V. K., and Menon, S., *Combust. Sci. Technol.* 162:175 (2001).
10. Kim, W. W., and Menon, S., *Combust. Sci. Technol.* 160:119–150 (2000).
11. Chen, Y. C., Peters, N., Schneemann, G. A., Wruck, N., Renz, U., and Mansour, M. S., *Combust. Flame* 107:233–244 (1996).
12. Borghi, R., "On the Structure and Morphology of Turbulent Premixed Flames," in *Recent Advances in the Aerospace Science* (C. Casci, ed.), Plenum, New York, 1985, pp. 117–138.
13. Pitsch, H., and Duchamp de Lageneste, L., "A G-Equation Formulation for Large-Eddy Simulation of Premixed Turbulent Combustion," CTR Annual Research Briefs, in press, 2002.
14. Peters, N., *Turbulent Combustion,* Cambridge University Press, Cambridge, U.K., 2000.
15. Moin, P., Squires, K., Cabot, W., and Lee, S., *Phys. Fluids A* 3:2746–2757 (1991).
16. Damköhler, G., *Z. Elektrochem.* 46:601–652 (1940).
17. Pitsch, H., and Steiner, H., *Phys. Fluids* 12(10):2541–2554 (2000).
18. Pierce, C. D., and Moin, P., AIAA paper 98-2892.
19. Pierce, C. D., "Progress-Variable Approach for Large Eddy Simulation of Turbulent Combustion," Ph.D. thesis, Stanford University, Stanford, CA, 2001.
20. Akselvoll, K., and Moin, P., *J. Fluid Mech.* 315:387–411 (1996).
21. Bowman, C. T., Hanson, R. K., Davidson, D. F., Gardiner Jr., W. C., Lissianski, V., Smith, G. P., Golden, D. M., Frenklach, M., and Goldenberg, M., *Gri-mech 2.11.,* University of California–Berkeley, 1995, www.me.berkeley.edu/gri_mech/.
22. Sussman, M., Smereka, P., and Osher, S., *J. Comput. Phys.* 119:146–163 (1994).
23. Russo, G., and Smereka, P., *J. Comput. Phys.* 163:51–67 (2000).
24. Boersma, B. J., Brethouwer, G., and Nieuwstadt, F. T. M., *Phys. Fluids* 10(4):899–909 (1998).

COMMENTS

Yung-Cheng Chen, University of Sydney, Australia. How does the prediction compare with the experimental data for the turbulent flame brush thickness for flame F3 (Ref. [11] in the paper)? The initial velocity data for the pilot flame have also been measured and are available for comparison from the first author of Ref. [11]. Is there any plan in the future to compute the flame F2 in Ref. [11], which has a high turbulence level and a different behavior in the axial evolution of the turbulent flame brush thickness?

Author's Reply. We have not looked into the data for the turbulent flame brush thickness yet. We are currently simulating flame F2 and will then possibly move on to flame F1 to assess the applicability of the flamelet model near the limits of its formal validity. In the comparison of F2 and F3, we will discuss the predictions of the flame brush thickness.

•

Andrei Lipatnikov, Chalmers University of Technology, Sweden. Let us consider the simplest case of a statistically planar, one-dimensional, fully developed, turbulent flame that propagates in a statistically uniform and stationary mixture. Then, in the framework linked with the flame, equation 6 from your paper is reduced to

$$\bar{\rho}\tilde{u}\,\frac{d\tilde{G}}{dx} = \bar{\rho}S_t\left|\frac{d\tilde{G}}{dx}\right|$$

if the curvature term $\kappa = 0$. Taking into account the mass conservation equation, $\rho\tilde{u} = \rho_u S_t$ instead of $\bar{\rho}S_t$ in the right-hand side of equation 6 appears to be more appropriate. What do you think? Is this correction of importance? In addition, what is the value of ρ at the flame surface associated with $G(x, y, z, t) = \tilde{G}_0$?

Author's Reply. The equation you are suggesting would be correct in the Reynolds averaged sense. Equation 6 from the present paper is a spatially filtered equation for LES. Even if the flow is steady and planar in the mean, in a turbulent flow, these assumptions will not be instantaneously met, and all terms in equation 6 remain. The *G*-equation can be written in different forms, as long as the turbulent burning velocity specifies the propagation speed with respect to the location where the convective velocity is evaluated. It is evident that the *G*-equation as given by equation 6 is a kinematic relation independent of the density, which would not be the case if the turbulent burning velocity was multiplied with the unburned rather than the local filtered density. However, the velocity appearing in the convective term is actually an average conditioned on the instantaneous position of $\tilde{G}_0$. The modeling of this conditional velocity is described in the paper.